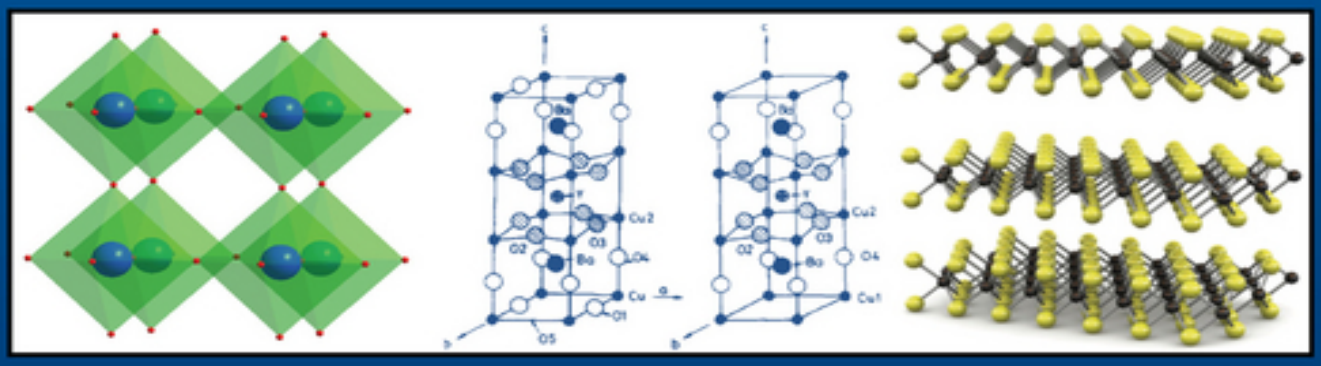

Essentials of
Inorganic Materials Synthesis

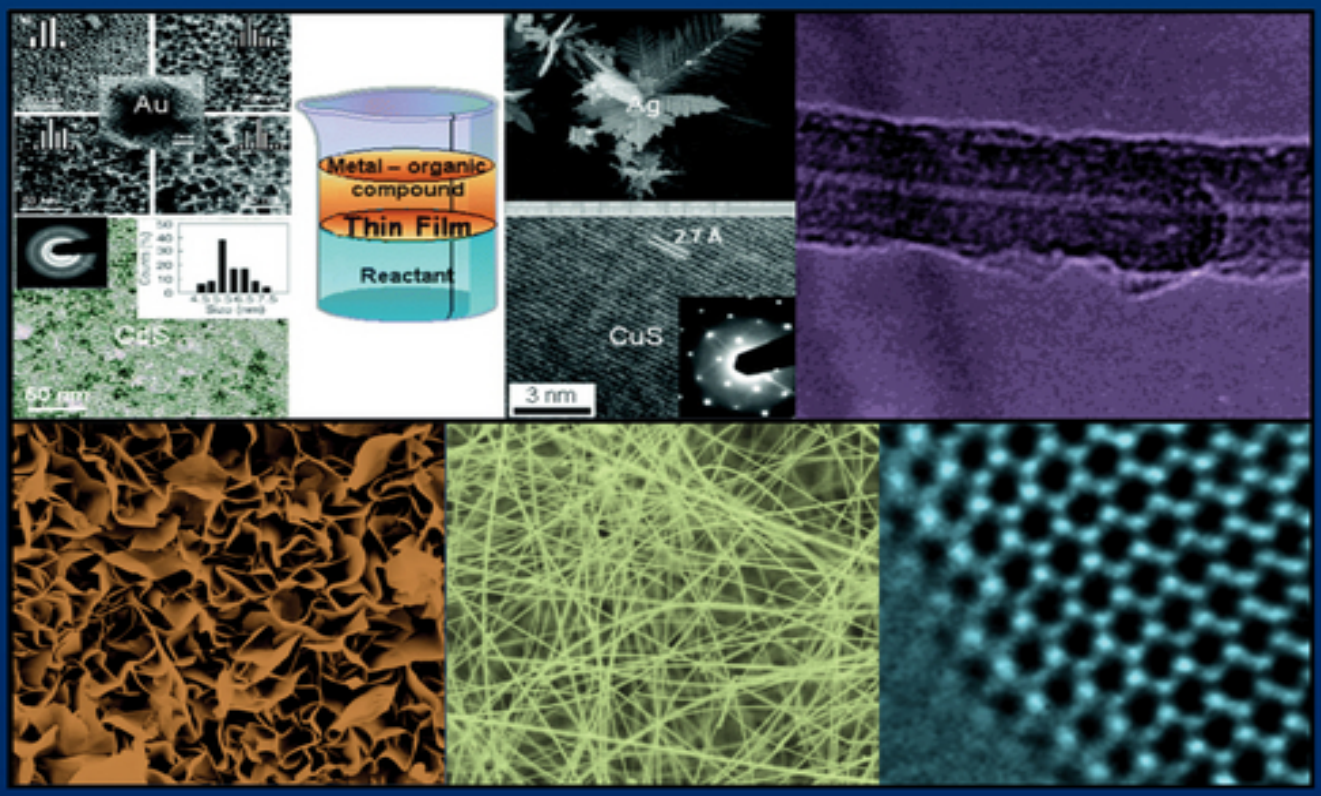

C. N. R. Rao • Kanishka Biswas

WILEY

CONTENTS

List of Tables

List of Illustrations

the NPs in perfluorocarbon (PFC) are also given as insets.

Figure 13.6 TEM images of (a) Au, (b) Ag, (c) CdS, and (d) CuS NPs formed at liquid–liquid interface.

Figure 13.7 (a, b) SEM and TEM images of the overall morphology of Au–Pd nanocubes self-assembled on the Si wafer and Cu grid, respectively. The dashed frames indicate the core area of particles. (c) Scanning transmission electron microscopy (STEM) images of the octahedral Au seed within a cubic Pd shell and cross-sectional compositional line profiles of a Au–Pd nanocube along the diagonal (indicated by a red line). (d) TEM image of an Au–Pd nanocube at high magnification. The inset is the SAED pattern taken from individual nanocubes.

Figure 13.8 TEM images of core–shell nanoparticles of (a) ReO_3–Au formed with a 5 nm ReO_3 particle. Inset shows ReO_3–Au formed over an 8 nm ReO_3 particle. (b) ReO_3–TiO_2 core–shell nanoparticle formed over a 32 nm ReO_3 particle with the inset showing a core–shell nanoparticle formed over a 12 nm ReO_3 nanoparticle. UV-visible absorption spectra of (c) ReO_3–Au core–shell nanoparticles (1:2 and 1:4). (d) ReO_3–TiO_2 core–shell nanoparticles (1:2 and 1:4) with a 12 nm ReO_3 particle.

Figure 13.9 (a) Schematic representation of VLS nanowire growth mechanism including three stages: (I) alloying, (II) nucleation and (III) axial growth. The three stages are projected onto (b) the conventional Au–Ge binary phase diagram to show the compositional and phase evolution during the nanowire growth.

Figure 13.10 In situ TEM images recorded during nanowire growth: (a) Au nanoclusters in the solid state at 500°C; (b) alloying initiated at 800°C, where Au exists mostly in the solid state; (c) liquid Au–Ge alloy; (d) nucleation of the Ge nanocrystal on the alloy surface; (e) elongation of the Ge nanocrystal with further Ge condensation, eventually forming (f) a wire.

Figure 13.11 TEM image of gold nanorods with aspect ratio ~25 obtained by solution-based reduction method making use of nanoparticle seeds.

Figure 13.12 (a, b) SEM images of zinc and cadmium nanowires obtained by the pyrolysis of the corresponding metal acetates at 1173 K. (c) TEM image of zinc nanowires and (d) TEM image of ZnO nanotubes obtained by the oxidation of Zn nanowires at 723 K.

Figure 13.13 (a) Crystal structure of *t*-Se showing a unit cell with helical chains of covalently bonded Se atoms extended along the *c*-axis. The growth direction of the one-dimensional nanostructures is shown along with an atomic model of a rod. (b) XRD patterns of the *t*-Se nanorods and bulk selenium powder used as the starting reagent. (c) SEM image of the Se nanorods obtained after 4 days by reacting 0.025 g of Se with 0.03 g of $NaBH_4$ in 20 ml water. (d) High-resolution electron microscopy (HREM) image of nanorods (arrow indicates the growth direction of the nanorods). (e) SEM image of *t*-Se scrolls obtained under hydrothermal conditions.

Figure 13.14 (a) Typical low-magnification TEM image of a ZnO nanohelix, showing its structural uniformity. (b) Low-magnification TEM image of a ZnO nanohelix with a larger pitch to diameter ratio.

The selected-area ED pattern (SAED, inset) is from a full turn of the helix. (c) Dark-field TEM image from a segment of a nanohelix. The edge at the right-hand side is the edge of the nanobelt. (d, e) High-magnification TEM image and the corresponding SAED pattern of a ZnO nanohelix with the incident beam perpendicular to the surface of the nanobelt, respectively, showing the lattice structure of the two alternating stripes. (f) Enlarged HRTEM image showing the interface between the two adjacent stripes.

Figure 13.15 (a, b) SEM images of the three-dimensional PbS nanowire array with an observable cubic seed (c) SEM image of units of the nanowire arrays prepared under a larger gas flow rate.

Figure 13.16 XRD patterns of (a) AlN, (b) GaN and (c) InN nanowires (asterisk indicates peaks arising due to substrate or gold). SEM images of (d) AlN, (e) GaN, (f) InN nanowires.

Figure 13.17 (a) Star-shaped PbSe nanocrystals and (b, c) radially branched nanowires. (d) TEM image of the (100) view of the branched nanowire and the corresponding selected-area electron diffraction pattern. (e) TEM image of the (110) view of the branched nanowire and the corresponding selected-area electron diffraction pattern.

Figure 13.18 (a) Schematic cross-sectional image of InP/InAs/InP core–multishell nanowire. (b) SEM image of periodically aligned InP/InAs/InP core–multishell nanowire array. (c) SEM image showing highly dense ordered arrays of core–multishell nanowires. Schematic illustration and high-resolution SEM cross-sectional image of a typical core–multishell nanowire observed after anisotropic dry

Transmission electron microscopy (TEM) images of various transition metal phosphide nanorods

Figure 14.5.1 Different types of intergrowth structures formed by the Aurivillius family of bismuth oxides. Notice the intergrowth of (1, 2), (2, 3) and (3, 4) layered units.

Figure 14.5.2 HRTEM of (3, 4) intergrowth structures: (a) $Bi_9Ti_6CrO_{27}$ involving the Aruivillius phases $Bi_4Ti_3O_{12}$ ($n = 3$) and $Bi_5Ti_3CrO_{15}$ ($n = 4$) and (b) $BaBi_8Ti_7O_{27}$. Computer-simulated images and unit cell lengths are shown.

Figure 14.5.3 Schematic drawing of (1, 4), (1, 5) and (1, 6) ITB. Hexagonal tunnels of HTB strips separate the WO_3 slabs shown in the polyhedral unit.

Figure 14.5.4 HRTEM of Bi_xWO_3 intergrowth bronze. The dark circles between the WO_3 slabs represent Bi atoms.

Figure 14.5.5 HRTEM of $MYMY_6$ intergrowth in barium ferrite: M = $BaFe_{12}O_{19}$; Y = $Ba_2Me_2Fe_{12}O_{22}$ (Me = Zn, Ni or Mg).

Figure 14.5.6 Schematic representation of (a) the structure of the $(MX)_{1+y}(TX_2)$ misfit compound, (b) the structure of the $(MX)_{1+y}(TX_2)$ misfit compound at initiation of the bending, and (c) formation of the tubular structure.

Figure 14.7.1 Superconducting $Bi_2CaSr_2Cu_2O_8$ and $Tl_2CaBa_2Cu_2O_8$.

Figure 14.7.2 Schematic structures of 123, 124 and 247 cuprates.

the cavities without touching the van der Waals atoms of the frameworks.

Figure 14.8.6 (a) Fusion of butlerite-type chains to form the layered structure in $M_2F_2(SO_4)_2(H_2O)_2]_n^{2n-}$, (M = Fe, Mn). (b) Layered in $[Fe_2^{III}Fe_3^{II}F_{12}(SO_4)_2(H_2O)_2]^4$ with symmetrical capping of the sulfate tetrahedra in the triangular lattice and the 10-membered aperture within it, redrawn from Ref. 33. (c) Polyhedral view of the kagome layer in $[HN(CH_2)_6NH][Fe^{III}Fe_2^{II}F_6(SO_4)_2][H_3O]$.

ESSENTIALS OF INORGANIC MATERIALS SYNTHESIS

C.N.R. RAO
KANISHKA BISWAS
International Center for Materials Science & New Chemistry Unit
Jawaharlal Nehru Centre for Advanced Scientific Research
Bangalore, India

WILEY

Published by John Wiley & Sons, Inc., Hoboken, New Jersey
Published simultaneously in Canada

Library of Congress Cataloging-in-Publication Data:

Rao, C.N.R. (Chintamani Nagesa Ramachandra), 1934– author.
Essentials of inorganic materials synthesis / C.N.R. Rao, Kanishka Biswas.
pages cm
Includes bibliographical references and index.

ISBN 978-1-118-83254-7 (hardback)
1. Inorganic compounds–Synthesis. I. Biswas, Kanishka, author. II. Title.
QD156.R36 2014
541′.39–dc23

2014035381

AUTHOR BIOGRAPHIES

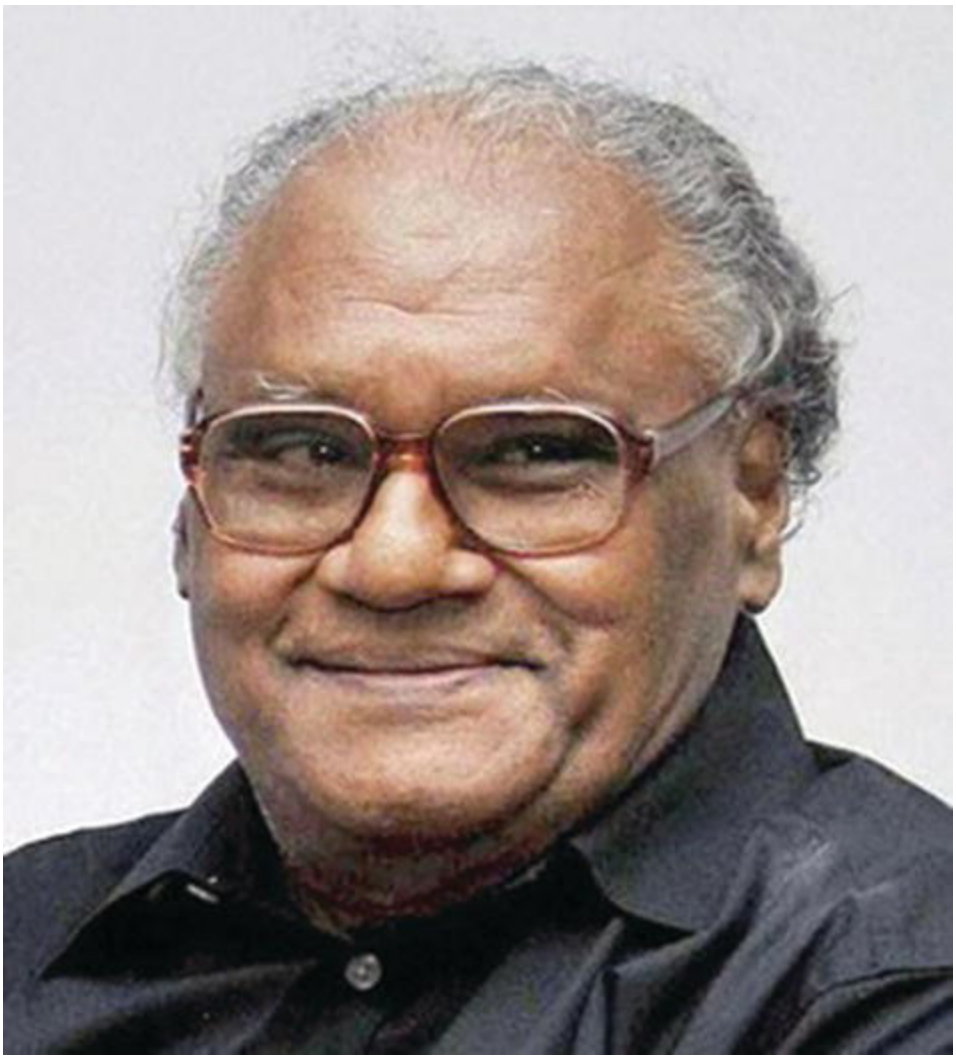

C.N.R. Rao obtained his Ph.D. degree from Purdue University (1958) and D.Sc. degree from the University of Mysore (1961). He is the National Research Professor and Linus Pauling Research Professor at the Jawaharlal Nehru Centre for Advanced Scientific Research and Honorary Professor at the Indian Institute of Science (both at Bangalore). His research interests are mainly in the chemistry of materials. He is a fellow of the Royal Society, London, a foreign associate of the US National Academy of

Sciences and a member of many other science academies. He is the recipient of the Einstein Gold Medal of UNESCO, the Hughes and Royal Medals of the Royal Society, the August Wilhelm von Hofmann medal of the German Chemical Society, the Dan David Prize and the Illy Trieste Science prize for materials research and the first India Science Prize.

Kanishka Biswas obtained his Ph.D. degree from Solid State Structural Chemistry Unit, Indian Institute of Science, India (2009), and did his postdoctoral research from Department of Chemistry, Northwestern University, USA (2009–2012). He is now a Assistant Professor (Faculty Fellow) in the New Chemistry Unit of Jawaharlal Nehru Centre for Advanced Scientific Research, Bangalore, India. He is an Associate of Indian Academy of Sciences,

Bangalore. He is pursuing research in solid-state chemistry of metal chalcogenides and thermoelectric ‘waste heat to electrical energy conversion’.

PREFACE

Chemical methods of synthesis play a crucial role in designing and discovering novel materials, especially metastable ones which cannot be prepared otherwise. They often provide better and less cumbersome methods for preparing known materials. There is a tendency nowadays to avoid brute-force methods and instead employ methods involving mild reaction conditions. Soft-chemistry routes are indeed becoming popular and will continue to be pursued greatly in the future. In view of the increasing importance of materials synthesis, we considered it appropriate to provide a proper account of the chemical methods of synthesis of inorganic materials in a book.

John Wiley had published a small monograph written by the first author of this book entitled *Chemical Approaches to the Synthesis of Inorganic Materials* some years ago (1994). We felt the need for a book which was more complete and yet handy, covering most of the synthetic methods employed by chemists and materials scientists. We believe that the present work answers such a need.

In this book, we briefly examine the different types of reactions and methods employed in the synthesis of inorganic solid materials. Besides the traditional ceramic procedures, we discuss precursor methods, combustion method, topochemical reactions, intercalation reactions, ion-exchange reactions, alkali-flux method, sol–gel method, mechanochemical synthesis, microwave synthesis, electrochemical methods, pyrosol process, arc and skull methods and high-pressure methods. Hydrothermal and solvothermal syntheses are discussed separately and also in sections dealing with specific materials. Superconducting cuprates and intergrowth structures are

discussed in separate sections. Synthesis of nanomaterials is dealt with in some detail. Synthetic methods for metal borides, carbides, nitrides, fluorides, silicides, phosphides and chalcogenides are also outlined.

While this book is not expected to serve as a laboratory guide, it is our hope that it provides an up-to-date account of the varied aspects of chemical synthesis of inorganic materials and serves as a ready reckoner as well as a guide to students, teachers and practitioners. The key references cited in the monograph would help to obtain greater details of preparative procedures and related aspects.

Bangalore
2015

C.N.R. Rao
Kanishka Biswas

1
INTRODUCTION

Much chemical ingenuity is involved in the synthesis of solid materials [1–6] and this aspect of material science is getting increasingly recognized as a crucial component of the subject. Tailor-making materials of the desired structure and properties is the main goal of material science and solid-state chemistry, but it may not always be possible to do so. While one can evolve a rational approach to the synthesis of solid materials [7], there is always an element of serendipity, encountered not so uncommonly. A good example of an oxide discovered in this manner is $NaMo_4O_6$ (Fig. 1.1) containing condensed Mo_6 octahedral metal clusters [8]. This was discovered by Torardi and McCarley in their effort to prepare the lithium analogue of $NaZn_2Mo_3O_8$. Another chance discovery is that of the phosphorus–tungsten bronze, $Rb_xP_9W_{32}O_{112}$, formed by the reaction of phosphorus present in the silica of the ampoule, during the preparation of the Rb–WO_3 bronze [9]. Since the material could not be prepared in a platinum crucible, it was suspected that a constituent of the silica ampoule must have got incorporated. This discovery led to the synthesis of the family of phosphorus–tungsten bronzes of the type $A_xP_4O_8\ (WO_3)_{2m}$. Chevrel compounds of the type $A_xMO_6S_8$ (A = Cu, Pb, La etc.) shown in Figure 1.2 were also discovered accidentally [10].

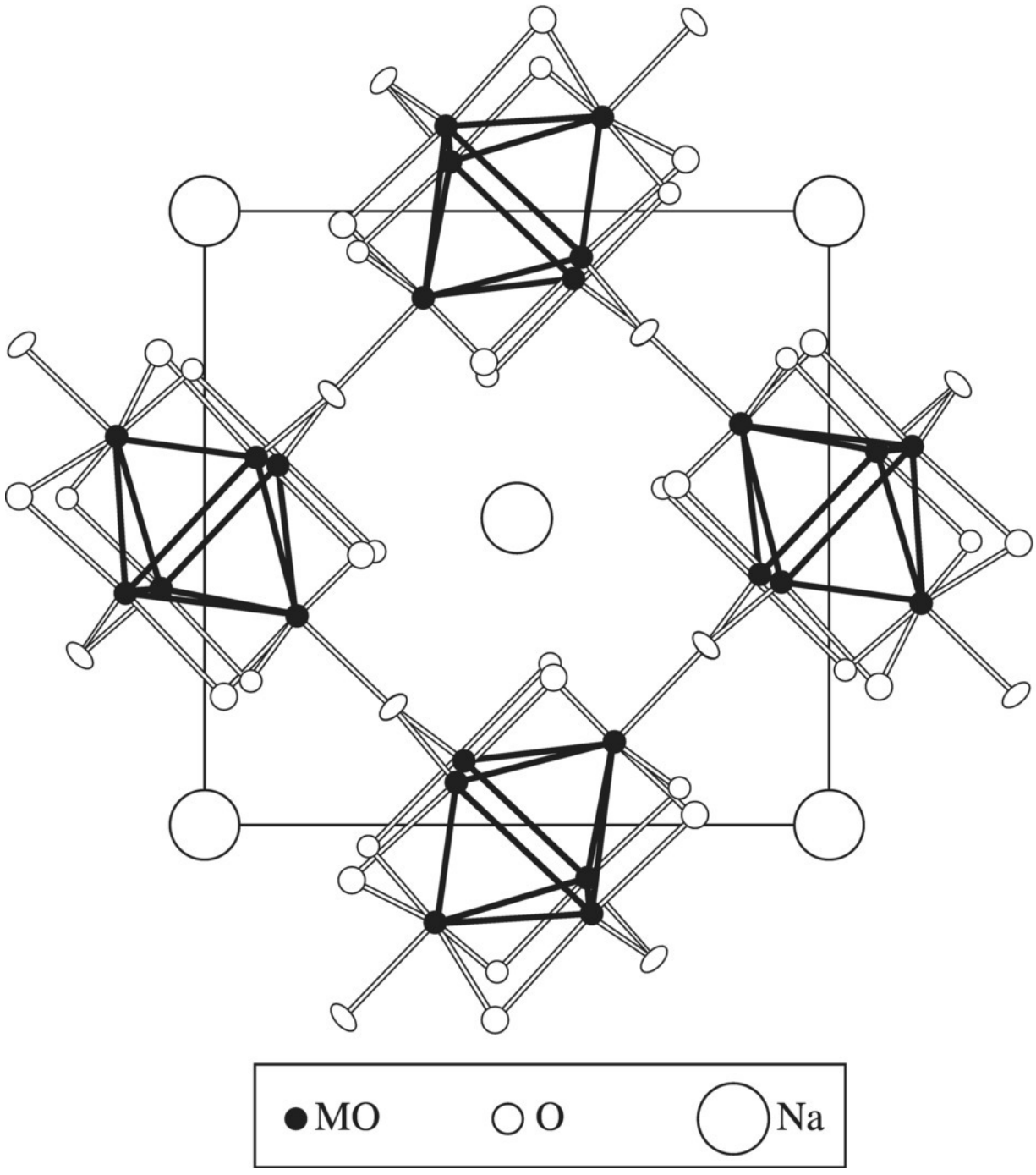

Figure 1.1 Structure of $NaMo_4O_6$.

(From Ref. 8, Torardi et al., *J. Am. Chem. Soc.*, **101** (1979) 3963. © 1979, American Chemical Society)

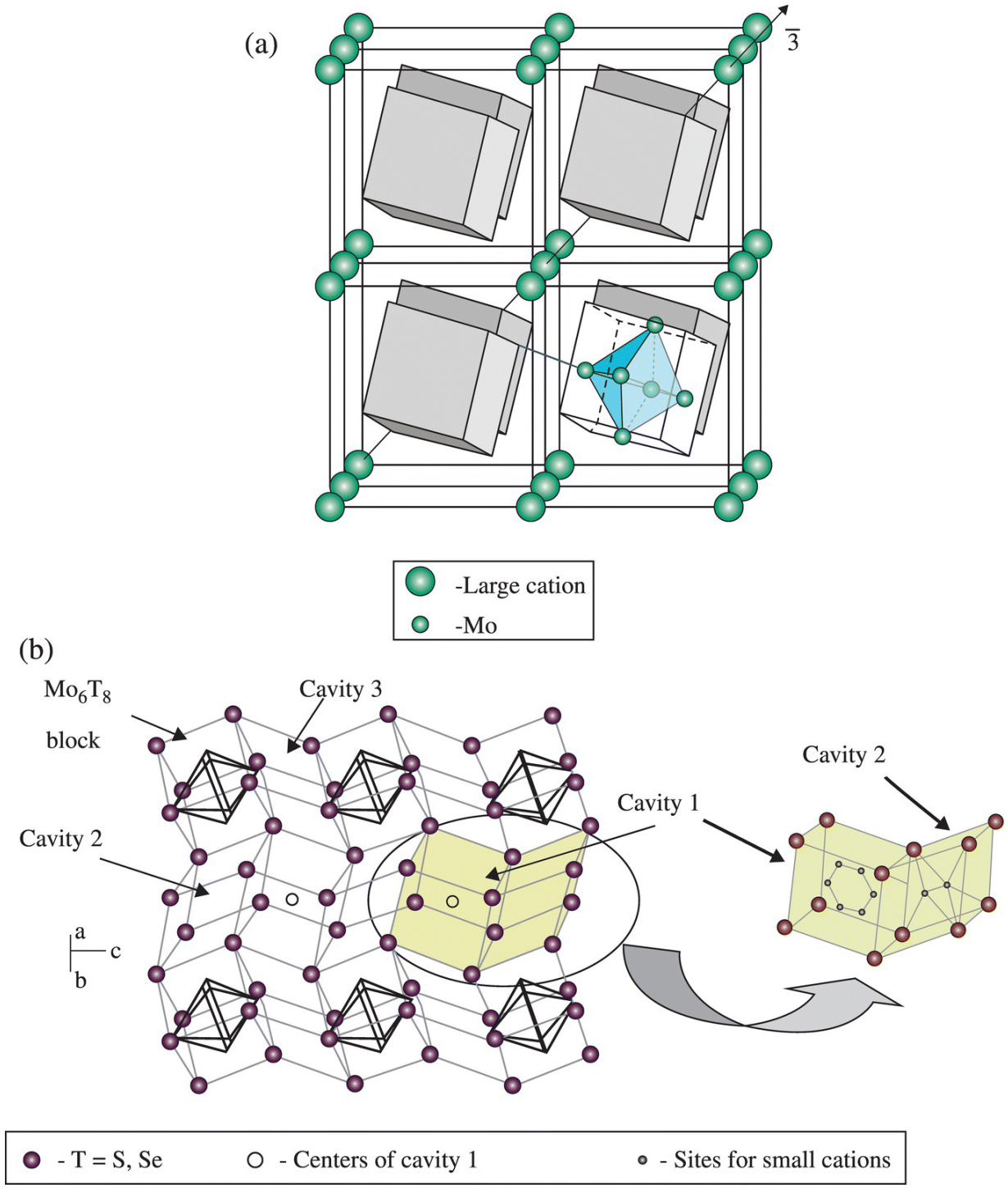
(a)
$\bar{3}$
-Large cation
-Mo
(b)
Mo_6T_8
block
Cavity 3
Cavity 2
Cavity 1
Cavity 2
a
c
b
- T = S, Se
- Centers of cavity 1
- Sites for small cations

Figure 1.2 Crystal structure of Chevrel phases. (a) Type I with large cation in the origin (eight rhombohedral unit cells): each cation is surrounded by eight Mo_6T_8 blocks. The internal structure is shown for one of the blocks. Intercluster Mo–T_1 bond is marked in blue. (b) Three types of pseudocubic cavities between the Mo_6T_8 blocks. Cavities 1 and 2 form the diffusion channels in three directions (a channel in one of the directions is shown here). Sites for small cations in cavities 1 and 2 are presented separately on the right.

Rational synthesis of materials requires knowledge of crystal chemistry besides thermodynamics, phase equilibria and reaction kinetics. There are several examples of rational synthesis. A good example is SIALON [11], where Al and oxygen were partly substituted for Si and nitrogen in Si_3N_4. The fast Na^+ ion conductor NASICON, $Na_3Zr_2PSi_2O_{12}$ (Fig. 1.3), was synthesized with a clear understanding of the coordination preferences of the cations and the nature of the oxide networks formed by them [12]. The zero-expansion ceramic $Ca_{0.5}Ti_2P_3O_{12}$ possessing the NASICON framework was later synthesized based on the idea that the property of zero-expansion would be exhibited by two or three coordination polyhedra linked in such a manner as to leave substantial empty space in the network [7]. Synthesis of silicate-based porous materials, making use of organic templates to predetermine the pore or cage geometries, is well known [13]. A microporous phosphate of the formula $(Me_4N)_{1.3}(H_3O)_{0.7}$ $Mo_4O_8(PO_4)_2{\cdot}2H_2O$, where the tretramethyl–ammonium ions fill the voids in the 3-dimensional structure made up of Mo_4O_8 cubes and PO_4 tetrahedra, has been prepared in this manner [14].

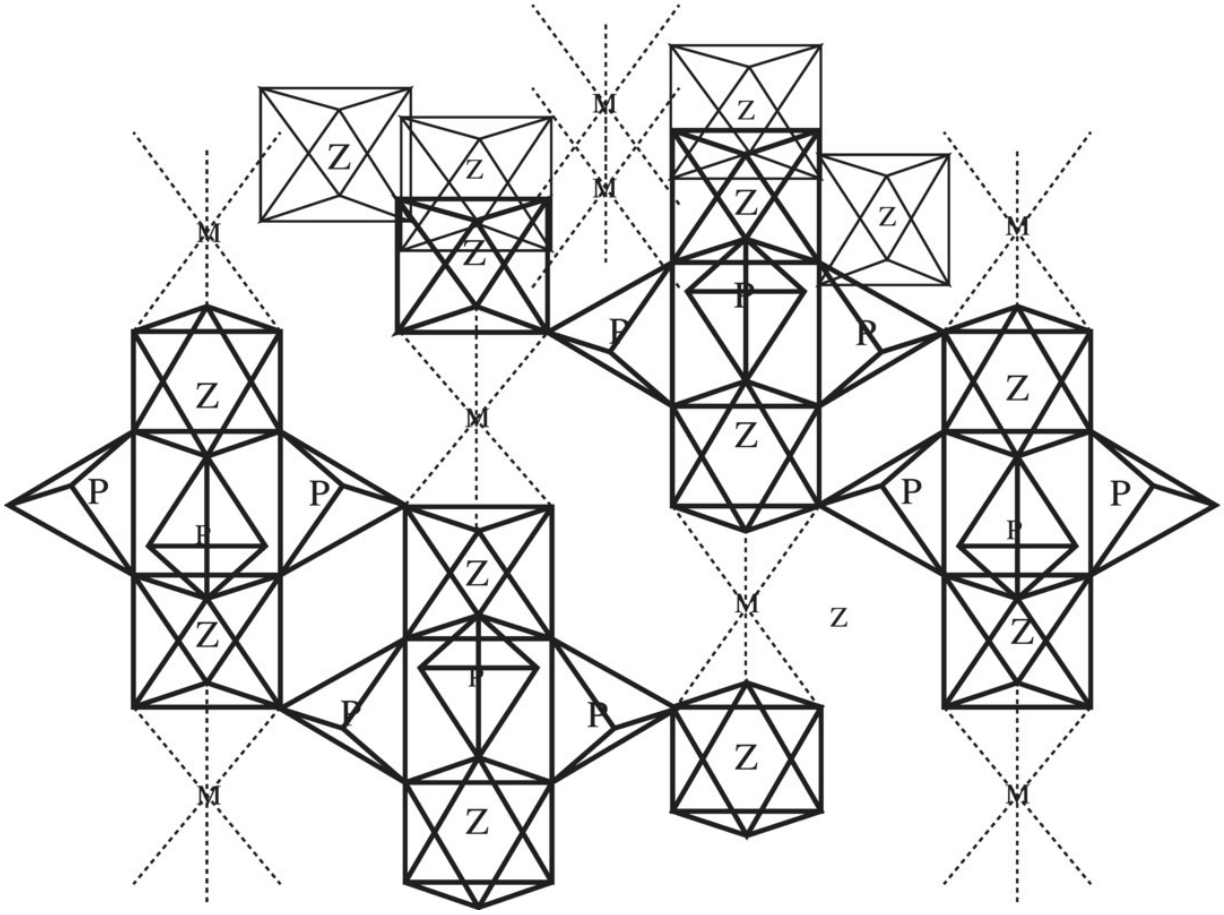

Figure 1.3 Structure of $NaZr_2(PO_4)_3$ which provided the design for NASICON: vacant trigonal–prismatic sites, p; octahedral Zr^{4+} sites, Z; and octahedral sites available for Na^+, M. For each M, there are three Mo sites forming hcp layers perpendicular to the *c*-axis.

A variety of inorganic solids have been prepared in the past several years by the traditional ceramic method, which involves mixing and grinding powders of the constituent oxides, carbonates and such compounds, and heating them at high temperatures with intermediate grinding when necessary. A wide range of conditions, often bordering on the extreme, such as high temperatures and pressures, very low oxygen fugacities and rapid quenching, have been employed in material synthesis. Low-temperature chemical routes and methods involving mild reaction conditions are,